

Robust Efficiency and Actuator Saturation Explain Healthy Heart Rate Control and Variability

Authors: Na Li^{1,*}, Jerry Cruz², Chenghao Simon Chien^{3,4}, Somayeh Sojoudi⁵, Ben Recht⁶, David Stone⁷, Marie Csete⁸, Daniel Bahmiller², John C. Doyle^{2,3,9}

Affiliations:

¹Laboratory of Information and Decision Systems, Massachusetts Institute of Technology, Cambridge, MA

²Department of Computing and Mathematical Science, California Institute of Technology, Pasadena, CA

³Department of Electrical Engineering, California Institute of Technology, Pasadena, CA

⁴Advanced Algorithm Research Center, Philips Healthcare, Thousand Oaks, CA

⁵Department of Neurology, NYU Comprehensive Epilepsy Center, NYU School of Medicine, New York, NY

⁶Electrical Engineering and Computer Sciences, University of California, Berkeley, CA

⁷Departments of Anesthesiology and Neurosurgery and the Center for Wireless Health, University of Virginia School of Medicine, Charlottesville, VA

⁸Huntington Medical Research Institutes, Pasadena, CA

⁹Department of BioEngineering, California Institute of Technology, Pasadena, CA

* To whom correspondence should be addressed. E-mail: na_li@mit.edu

Key words:

Heart rate variability, robust efficiency, actuator saturation, system identification, optimal control

Significance Statements

Reduction in human heart rate variability (HRV) is recognized in both clinical and athletic domains as a marker for stress or disease, but previous mathematical and clinical analyses have not fully explained the physiological mechanisms of the variability. Our analysis of HRV employing the tools of control mathematics reveals that the occurrence and magnitude of observed HRV is an inevitable outcome of a controlled system with known physiological constraints. In addition to a deeper understanding of physiology, control analysis may lead to the development of timelier monitors that detect control system dysfunction, and more informative monitors that can associate HRV with specific underlying physiological causes.

Abstract:

The correlation of healthy states with heart rate variability (HRV) using time series analyses is well documented. While these studies note the accepted proximal role of autonomic nervous system (ANS) balance in HRV patterns, the responsible deeper physiological (and clinically relevant) mechanisms have not been fully explained. Using mathematical tools from control theory, we combine mechanistic models of basic physiology with experimental data from human subjects to explain causal relationships among states of stress vs. health, HR control, and HRV, and more importantly, the physiologic requirements and constraints underlying these relationships. Nonlinear dynamics play an important explanatory role- most fundamentally in the actuator saturations arising from unavoidable tradeoffs in robust homeostasis and metabolic efficiency. While mathematical models and tools are essential for our results and for optimal clinical interpretation of HR data, we also provide simple and intuitive physiological explanations for HR control and HRV. All these results are grounded in domain-specific mechanisms, tradeoffs, and constraints, but they also illustrate important, universal properties of complex systems. We show that the study of complex biological phenomena like HRV requires a framework which facilitates inclusion of diverse domain specifics (e.g. due to physiology, evolution, and measurement technology) in addition to general theories of efficiency, robustness, feedback, dynamics, and supporting mathematical tools.

Introduction

Biological systems display a variety of well known rhythms in physiological signals [1-6], with particular patterns of variability associated with a healthy state [2-6]. Decades of research demonstrates that heart rate (HR) in healthy humans has high variability, and loss of this high HR variability (HRV) is correlated with adverse states such as stress, fatigue, physiologic senescence, or disease [6-12]. The dominant approach to analysis of HRV has been to focus on statistics and patterns in HR time series that have been interpreted as fractal, chaotic, scale-free, critical, etc. [6-15]. The appeal of time series analysis is understandable as it puts HRV in the context of a broad and popular approach to complex systems [16], and claims connection of HRV to clinically relevant outcomes [5], all while requiring minimal attention to domain-specific (e.g. physiological) details. Yet despite intense research activity in this area, there is limited consensus regarding causation or mechanism and minimal clinical application of the observed phenomena [10].

Increasingly, multidisciplinary experts who are otherwise enthusiastic about the broader applicability of chaos and fractals question their relevance to HRV [17], and question even the most basic claims regarding correlations with health and disease [18]. This trend is consistent with a broader critique on the lack of statistical and methodological rigor on complex systems in science and medicine generally [19-22]. This paper takes a completely different approach, aiming for more fundamental rigor and potential clinical relevance. We offer simple physiological explanations for the largest source of HRV and its changes, as well as methods that help systematically pursue such explanations.

Fig. 1 shows the type of HR data analyzed, collected from healthy young athletes (n=5). The data display responses to changes in muscle work rate on a stationary bicycle during mostly aerobic exercise. **Fig. 1A** shows 3 separate exercise sessions with identical watts fluctuations about 3 different means. With proper sleep, hydration, nutrition, and prevention from overheating, trained athletes can maintain the highest workload in **Fig. 1** for hours and the lower and middle levels almost indefinitely. This ability requires *robust efficiency*: high workloads are sustained while robustly maintaining metabolic homeostasis, a particularly challenging goal in the case of the relatively large, metabolically demanding, and fragile human brain.

While mean HR in **Fig. 1A** increases monotonically with workloads, both slow and fast fluctuations (i.e. HRV) in HR are saturating nonlinear functions of workloads, meaning that both high and low frequency HRV component goes down. Results from all subjects showed qualitatively similar nonlinearities (see SI). We will argue that this *saturating nonlinearity* is the simplest and most

fundamental example of change in HRV in response to stressors [11, 12, 23] (exercise in the experimental case, but in general also fatigue, dehydration, trauma, infection, even fear and anxiety [6-9, 11, 12, 23]).

Physiologists have correlated HRV and autonomic tone [7, 11-13], and the (im)balance between sympathetic stimulation and parasympathetic withdrawal [12, 24-26]. The alternation in autonomic control of HR (more sympathetic and less parasympathetic tone during exercise) serves as an obvious proximate cause for *how* the HRV changes as shown in **Fig. 1**, but the ultimate question remains as to *why* the system is implemented this way. It could be an evolutionary accident, or could follow from hard physiologic tradeoff requirements on cardiovascular control, as work in other systems suggests [1]. Here, the explanation of HRV similarly involves hard physiological tradeoffs in robust efficiency and employs the mathematical tools necessary to make this explanation rigorous in the context of large measurement and modeling uncertainties.

Physiological tradeoffs

The central physiological tradeoffs in cardiovascular control [25-30], shown schematically in **Fig. 2**, involve interconnected organ systems and four types of signals that are very different in both functional role and time series behavior, but together define the requirements for robust efficiency of the cardiorespiratory system. The main control requirement is to maintain 1) small, acceptable “errors” in internal variables for brain homeostasis (e.g., cerebral blood flow CBF, arterial O_2 saturation SaO_2) and efficient working muscle O_2 utilization (ΔO_2) using 2) actuators (heart rate H , minute ventilation \dot{V}_E , vasodilation and systemic peripheral (vascular) resistance (R_s) and brain autoregulation) in response to 3) external disturbances (workload W), and 4) internal sensor noise and perturbations (e.g. pressure changes from different respiratory patterns due to pulsatile ventilation V).

In healthy fit subjects, keeping errors in CBF, SaO_2 , and ΔO_2 suitably small while responding to large, fast variations in W disturbance necessitates compensating and coordinated changes in actuation via responses in H , \dot{V}_E , R_s , and cerebral autoregulation. Thus healthy response involves low error but high control variability whereas loss of health is exactly the opposite. We will show that the observed striking changes in HRV such as those seen in **Fig. 1** result from tradeoffs between these errors combined with various actuator saturations.

A challenge to this approach lies in managing the necessary but potentially bewildering complexity inherent in the physiological details, mathematical methods, and measurement technology. To achieve this, we make each small step in the analysis as simple, accessible, and reproducible as

possible from analysis of experimental data to modeling to physiological and control theoretic interpretation. In addition, we restrict the physiology (shown schematically in **Fig. 2**) [25-30] and control theory [30-33] to basic levels and all software is standard and open source. We also make several passes through the analysis and modeling with increasing complexity, sophistication, and depth, to aid intuition while highlighting the need for rigorous, scalable methods.

In addition to mechanistic physiological models, we also use systems identification techniques (referred to as black-box *fits* in this paper) [23, 31, 34, 35] as intermediate steps to identify parsimonious canonical dynamical input-output models relating HR as an output variable to input disturbances such as workload and ventilation. These techniques establish causal deterministic links between input and output variables; highlight the aspects of time series and dynamic relationships that are explored further; and give some indication of the degree of complexity of their dynamics. Then, we use physiologically motivated models (referred to as first-principle *models* in this paper) [27-30] to study the mechanisms that drive the dynamics. The two approaches are complementary: Black-box fits highlight essential relationships that may be hard to intuit from data alone and can be obscured in both complex data sets and mechanistic models, while first-principles models give physiological interpretations to these dynamical relationships.

Results

Static Fits

Table 1 lists the minimum root mean square (RMS) error $\|H_data-H_fit\|$ (where $\|x\| \triangleq \sqrt{\sum_{t=1}^N (x_t)^2} / N$ for a time series x_t of length N) for several static and dynamic fits of increasing complexity for the data in **Fig. 1**. Not surprisingly, **Table 1** shows that the RMS error becomes roughly smaller with increased fit complexity (in terms of the number of parameters). Rows 2 and 5 of Table 1 (in blue) are single global linear fits for all the data, while the remaining rows (in white) have different parameters for each cell and are thus *piecewise* linear when applied to all the data. The “best” piecewise linear models balancing error with complexity are further highlighted in yellow in **Table 1**.

We will initially focus on static linear fits (first 4 rows) of the form $h(W)=b \cdot W+c$, where b and c are constants that minimize the RMS error $\|H_data-h(W)\|$, which can be found easily by linear least squares. Static models have limited explanatory power but are simple starting points in which constraints and tradeoffs can be easily identified and understood, and we use only methods that directly generalize to dynamic models (showed later) with modest increase in complexity. Row 1 of **Table 1** is

the trivial “zero” fit with $b=c=0$; Row 2 is the best global linear fit with $(b,c)=(0.35,53)$ which is used to linearly scale the units of W (blue) to best fit the HR data (red) in **Fig. 1A**; Row 3 is a piecewise constant fit with $b=0$ and c being the mean of each data set; Row 4 is the best piecewise linear fits (black dashed lines in **Fig. 1A**) with quite different values (b,c) of $(0.44,49)$, $(0.14,82)$ and $(0.04,137)$ at 0-50, 100-150, and 250-300 watts. The piecewise linear model has less error than the global linear fit. At high workload level, HR in **Fig. 1** does not reach steady state on the time scale of the experiments, the linear static fit is little better than constant fit, and so these data are not considered further for static fits and models.

Both **Table 1** and **Fig. 1** imply that HR responds somewhat nonlinearly to different levels of workload stressors. The solid black curve in **Fig. 3A** shows idealized (i.e. piecewise linear) and qualitative but typical values for $h(W)$ globally that are consistent with the static piecewise linear fits at the two lower watts levels in **Fig. 1A**. The change in slope of $H=h(W)$ with increasing workload is the simplest manifestation of changing HRV and is now our initial focus. A proximate cause is autonomic nervous system (ANS) balance, but we are looking for a deeper *why* in terms of whole system constraints and tradeoffs.

Static Models

As we mentioned earlier, in healthy fit subjects, the central physiological tradeoffs in cardiovascular control requires keeping errors such as CBF, SaO_2 , and ΔO_2 suitably small in response to variations in W disturbance through changes in actuations such as H . To better understand the tradeoff, we derive a steady state model $(P_{as}, \Delta O_2) = f(H, W)$ from standard physiology that constrains the relationship between $(P_{as}, \Delta O_2)$ and (H, W) independent of how H is controlled (details below). Here P_{as} is mean systemic arterial blood pressure (MAP), which is an important variable affecting the CBF [26, 36] and ΔO_2 is the drop in oxygen content across working muscle (Notice that the model already assumes constant SaO_2 , which is consistent with data measurement and literature [25].). The mesh plot in **Fig. 3C** is the image on the $(P_{as}, \Delta O_2)$ plane of the **Fig. 3B** (H, W) mesh plot under this function $f(H, W)$ for generic, plausible values of physiological parameters. Thus any function $H=h(W)$, can be mapped from the (H, W) plane using model $(P_{as}, \Delta O_2) = f(H, W)$ to the $(P_{as}, \Delta O_2)$ plane to determine its consequences for the most important tradeoffs, which involve P_{as} and ΔO_2 . These results are shown with the black lines in **Fig. 3B**, that give $H=h(W)$ curves consistent with **Fig. 3A** and then are mapped onto **Fig. 3C**.

Hidden complexity is unavoidable in the model $(P_{as}, \Delta O_2) = f(H, W)$, but we temporarily defer these details to focus on the general shape of the color-coded curves in **Fig. 3B-C**, which have an intuitively clear explanation highlighted by the dashed red and purple lines. At constant workload, increased HR would greatly increase P_{as} while slightly decreasing ΔO_2 due to greater flow rate through the muscle. For constant HR, increased workload would greatly increase ΔO_2 while slightly reducing P_{as} due to greater oxygenation and peripheral vasodilatation. The cardiovascular control system adjusts HR as a function $H=h(W)$ of workload to trade off increasing P_{as} with increasing ΔO_2 , both of which are undesirable. This tradeoff in robust efficiency and how it changes at different HR levels are the essential sources of the nonlinearities in the solid black lines in **Fig. 3**, with relatively small nonlinearity in the function $(P_{as}, \Delta O_2) = f(H, W)$ manifested in modest curvature of the colored meshes in **Fig. 3C**.

The hypothetical linear response at low workload in **Fig. 3** can be explained in terms of purely metabolic tradeoffs. Healthy athletes can maintain the low workload almost indefinitely even in adverse (e.g. heat) conditions, a feature of human physiology thought to be an important adaptation for a successful hunter [37]. Prolonged exercise necessarily requires steeply increased HR to provide sufficient tissue O_2 (low ΔO_2), to maintain aerobic lipid metabolism in muscles and preserve precious carbohydrates for the brain.

The nonlinear response in **Fig. 3** (solid lines) reflects additional tradeoffs that arise at higher workload and HR, when the resulting high P_{as} becomes dangerous mainly due to actuator saturation of cerebral autoregulatory control. In healthy humans, CBF is autoregulated to be quite constant [26, 36] over a relatively wide range of P_{as} ($50 < P_{as} < 150$ mm Hg), so that no new tradeoffs at moderate exercise levels are required, because P_{as} is within this range. A new tradeoff does arise at P_{as} above 150 mm Hg when cerebral autoregulation saturates, and CBF begins to rise with the severe possible consequences of edema and/or hemorrhage.. Thus for the dashed black linear response in **Fig. 3B-C**, the resulting P_{as} would be elevated to potentially pathologic levels, and some nonlinearity as in the solid black line is necessary. Moreover, in many subjects there may be diminishing metabolic benefit of high tissue O_2 (low ΔO_2) at high workloads because muscle mitochondria saturate. While many details of cerebral autoregulation (as well as the mitochondrial saturation) are poorly understood, the P_{as} at which autoregulation saturates is well-known in healthy adults, and helps to explain an important change in HRV with stressors. Ultimately, cardiac output itself saturates at sufficiently high HR due to compromised diastolic filling time with subsequent dramatic falls in stroke volume.

Mathematically, all these factors can be quantitatively reflected in a static optimization model using linear least squares, with $H=h(W)$ chosen to minimize a weighted penalty on increasing P_{as} , ΔO_2 and H :

$$\min q_P^2 (P_{as} - P_{as}^*)^2 + q_{O_2}^2 (\Delta O_2 - \Delta O_2^*)^2 + q_H^2 (H - H^*)^2$$

subject to linearization of the constraint $(P_{as}, \Delta O_2) = f(H, W)$ at 0 and 100 watts. Here $P_{as}^*, \Delta O_2^*, H^*$ are the steady values for $P_{as}, \Delta O_2, H$ at 0 and 100 watts respectively. Different values for (q_P, q_{O_2}, q_H) reflect different tradeoffs between P_{as} , ΔO_2 , and H at different workloads. In particular, q_P is higher at high watts and high HR, reflecting the greater impact of P_{as} on CBF due to saturation of autoregulation, and q_H is higher to reflect the saturation of HR itself, which becomes more acute at higher watts levels. Straightforward, standard computations easily reproduce the piecewise linear features in **Fig. 3** with higher penalty on P_{as} and H at higher workload levels.

An important feature of this approach is that it allows systematic exploration of models that are both simple and explanatory. We have systematically moved from the data in **Fig. 1** to the fit in **Fig. 3A**, and then from very simple well understood physiological mechanisms to how healthy HR should behave and be controlled, reflected in **Fig 3B-C**. The nonlinear behavior of HR is explained by combining explicit constraints in the form $(P_{as}, \Delta O_2) = f(H, W)$ due to well-understood physiology with constraints on homeostatic tradeoffs between rising P_{as} and ΔO_2 that change as W increases. The physiologic tradeoffs depicted in these models explain *why* a healthy neuroendocrine system would necessarily produce changes in HRV with stress, no matter *how* the remaining details are implemented. Taken together this could be called a “grey box” model since it combines hard physiological constraints both in $(P_{as}, \Delta O_2) = f(H, W)$ and homeostatic tradeoffs to derive a resulting $H=h(W)$. If new tradeoffs not considered here are found to be significant, they can be added directly to the model as additional constraints, and solutions recomputed. The ability to include such physiological constraints and tradeoffs is far more essential to our approach than what is specifically modeled (e.g. that primarily metabolic tradeoffs at low HR shift priority to limiting P_{as} as cerebral autoregulation saturates at higher HR). This extensibility of the methodology will be emphasized throughout.

The most obvious limit in using static models is that they assume HR responds instantaneously to workloads, so important transient dynamics in HR are ignored, missing what is arguably the most striking manifestations of changing HRV seen in **Fig. 1**. Fortunately, our method combining data fitting,

first principles modeling, and constrained optimization readily extends beyond static models. The tradeoffs in robust efficiency in P_{as} and ΔO_2 that explain changes in HRV at different workloads also extend directly to the dynamic case as demonstrated later.

Dynamic Fits

In this section we extract more dynamic information from the exercise data. The fluctuating perturbations in workload (**Fig. 1**) imposed on a constant background (stress) are targeted to expose essential dynamics, first captured with “black-box” input/output dynamic versions of above static fits. **Fig. 1B** shows the simulated output $h(t) = \text{HR}$ (in black) of simple local (piecewise) linear dynamics (with discrete time t in seconds)

$$\Delta h(t) = h(t+1) - h(t) = a h(t) + b W(t) + c \quad (1)$$

where the input is $W(t) = \text{workload}$ (blue). Constants (a, b, c) are fit to minimize the RMS error between $h(t)$ and HR data as before (**Table 1**). The optimal parameter values $(a, b, c) \approx (-0.22, 0.11, 10)$ at 0 watts differ greatly from those at 100 watts $(-0.06, 0.012, 4.6)$ and at 250 watts $(-0.003, 0.003, -0.27)$, so a single model equally fitting all workload levels is necessarily nonlinear. This conclusion is confirmed by simulating HR (blue in **Fig. 1B**) with one best global linear fit $(a, b, c) \approx (0.06, 0.02, 2.93)$ to all three exercises, which has large errors at high and low workload levels.

The changes of the large, slow fluctuations in both HR (red) and its simulation (black) in **Fig. 1B** are consistent with well-understood cardiovascular physiology, and illustrate how the physiologic system has evolved to maintain homeostasis despite stresses, here those due to workloads. Our next step in modeling is to mechanistically explain as much of the HRV changes in **Fig. 1** as possible using only standard models of aerobic cardiovascular physiology and control [25-29]. This step focuses on the changes in HRV in the fits in **Fig. 1B** (in black) and equation (1) and we defer modeling of the high frequency variability in **Fig. 1** until later (i.e., the differences between the red data and black simulations in **Fig. 1B**).

The black box fits allow us to plausibly conjecture that workload disturbances cause most of the variability in **Fig. 1-B** (black curves). Here the rigor of the black-box fits is important, as highlighted by three features: 1) no comparably good fits exist for the data in **Fig. 1** without the input of workload, 2) within the limits of the sensors used and subject fitness we can otherwise experimentally manipulate the input independently and over a wide range to make it truly a “causal” input, and 3) the fits accurately predict the HR output response to new experiments (i.e. cross-validation, see SI).

First Principles Models

Our first principle model is based on the circulatory circuit diagram in **Fig. 2**, using standard mathematical descriptions of circulation, and with a focus on modeling purely aerobic exercise. That is, we only model blood flow, blood pressure, and O_2 in several compartments, and yet the model captures the overall physiologic HR response during moderate exercise in young, fit adults. In standard models of aerobic cardiovascular control [25-29] the neuroendocrine system controls peripheral vasodilation, minute ventilation, and cardiac output to maintain blood pressure and oxygen saturation within acceptable physiological limits.

Several features of these control systems allow substantial simplification of the model. Minute ventilation \dot{V}_E alone can tightly control arterial oxygenation $[O_2]_a$, so we assume $[O_2]_a$ is maintained nearly constant (consistent with the nearly constant oxygen saturation S_aO_2 throughout all the exercise [25], data not shown). Moreover, peripheral resistance R_s is decreased during exercise and the decrease is determined by local metabolic control. The purpose of decreasing R_s in the arterioles is to increase blood flow and regional delivery of O_2 , glucose, and other substrates as needed. Since the *venous* oxygenation $[O_2]_v$ serves as a good signal for oxygen consumption, we also assume that control of peripheral vascular resistance R_s is a function only of *venous* oxygenation $[O_2]_v$ [29].

Combined with those models for blood circulation and oxygen consumption, we have the following physiological model:

$$\begin{aligned}
V_{as} &= c_{as} \cdot P_{as} & Q_l &= c_l \cdot H \cdot P_{vp} \\
V_{vs} &= c_{vs} \cdot P_{vs} & Q_r &= c_r \cdot H \cdot P_{vs} \\
V_{ap} &= c_{ap} \cdot P_{ap} & F_s &= (P_{as} - P_{vs}) / R_s \\
V_{vp} &= c_{vp} \cdot P_{vp} & F_p &= (P_{ap} - P_{vp}) / R_p \\
V_{tot} &= V_{as} + V_{vs} + V_{ap} + V_{vp} & M &= \rho \cdot W + M_0 \\
[O_2]_a &= 0.2 & R_s &= A \cdot [O_2]_v + R_{s0}
\end{aligned} \tag{2}$$

Here V and P are (subscripts a =arterial, v =venous, s =systemic, p =pulmonary) blood volume and blood pressure respectively. All of the c variables are constants. The main elements of the model are (more details in SI): (i) arterial and venous compartments of systemic and pulmonary circulations are treated as compliant vessels, modeled in the form $V=c \cdot P$, with the total blood volume a constant V_{tot} ; (ii) cardiac output of the left (Q_l) and right (Q_r) ventricles; (iii) blood flow for systemic (F_s) and pulmonary (F_p) circulation; (iv) the metabolic consumption M ; (v) $[O_2]_a$ and R_s are modeled according to the previous description about the control mechanism. Note that we need not model these control systems in detail, but simply extract their most well-known features and use them to constrain the model.

In steady state the follow additional constraints hold:

$$\begin{aligned} Q_r &= Q_l = F_s = F_p \\ M &= F_s ([O_2]_a - [O_2]_v) \end{aligned} \quad (3)$$

The first equation is total blood circulation balance and the second one is based on the oxygen circulation balance, where $F_s([O_2]_a - [O_2]_v)$ is the net change in the arterial and venous blood O_2 content. The oxygen drop ΔO_2 across the muscle bed is defined as $\Delta O_2 = [O_2]_a - [O_2]_v$. Combining (2) and (3) plus simple algebra (see SI) gives the steady state model $(P_{as}, \Delta O_2) = f(H, W)$ shown in **Fig. 3** that constrains the relationship between $(P_{as}, \Delta O_2)$ and (H, W) .

In general the circulatory system is far from steady state in our experiments. Modeling the blood volume change for each circulatory compartment and the oxygen change in the tissue keeps the constraints from equation (2) but replaces (3) with the following dynamic model:

$$\begin{aligned} c_{as} \dot{P}_{as} &= Q_l - F_s \\ c_{vs} \dot{P}_{vs} &= F_s - Q_r \\ c_{ap} \dot{P}_{ap} &= Q_r - F_p \\ v_{T,O_2} [\dot{O}_2]_v &= -M + F_s \cdot ([O_2]_a - [O_2]_v) \\ c_{vp} P_{vp} &= V_{total} - (c_{as} P_{as} + c_{vs} P_{vs} + c_{ap} P_{ap}) \end{aligned} \quad (4)$$

Here v_{T,O_2} denotes the effective tissue O_2 volume and we assume that tissues and venous blood gases are in equilibrium, namely that tissue oxygenation $[O_2]_T$ is the same as venous oxygenation $[O_2]_v$ (see SI). The previous static analysis (and the purely static tradeoffs it highlights) directly extends to the dynamic case with modestly increased complexity. The simplest extension is to use an optimal linear quadratic (LQ) state feedback controller [32] for linearizations of (4) at 0 and 100 watts, with controller $H = u(\cdot)$ chosen to minimize a weighted penalty on integrated elevation of P_{as} , ΔO_2 and H :

$$\min \int \left(q_P^2 (P_{as} - P_{as}^*)^2 + q_{O_2}^2 (\Delta O_2 - \Delta O_2^*)^2 + q_H^2 (H - H^*)^2 \right) dt$$

subject to linearizations of the state dynamic constraint (4). **Fig. 4** compares HR and workload data versus simulations of such linear controllers (but using the nonlinear model) for two experiments (similar to **Fig. 1** but with a different subject) with higher penalty on P_{as} and H at higher workloads as in the static case. (See SI for more details.) Also shown are simulations of P_{as} and $[O_2]_T$, which are consistent with the literature but were not measured. The same methods and results apply to other subjects' data and new experiments (e.g. cross-validation, see SI).

The change in the tradeoff as workload increases is consistent with what we observed using the static model. At low workload and low HR, the main tradeoff is metabolic since both P_{as} and HR are at safe and sustainable levels. High HR and thus high $[O_2]_T$, (low ΔO_2), maintains aerobic muscle metabolism, extending the potential duration of exercise while preserving carbohydrate resources for the brain. At higher workloads, this strategy would produce unsustainably high and potentially damaging P_{as} and possibly HR, so the optimal controller penalizes these factors more, at the price of reduced $[O_2]_T$. HRV (slow time scale) in **Fig. 1** (and P_{as} in **Fig. 4**) decreases with increasing workload because of these straightforward but changing tradeoffs between metabolic overhead and P_{as} , ΔO_2 , and H as their means increase. Thus the explanations in HRV derived from the dynamic aerobic model are richer and more complete but due to the same tradeoffs as in the simpler static model.

Importantly, though the mathematics and physiology required are relatively elementary and the resulting explanation is intuitively clear and mechanistic, they nonetheless highlight the rigor and scalability of this approach. The simplicity of the “black box” fits in (1) and **Fig. 1** helps establish causal relationships between variables and suggests physiological mechanisms to model in more detail, and highlights features in the signals that are *not modeled* (i.e., we have not explained the high frequency of the signals at low watts in **Fig. 1**, considered in the next sections). The hard homeostatic tradeoffs and the actuator effects of HR, ventilation, and vasodilation were included in the physiology model in (2)-(4) but the neuroendocrine implementation details were not. Also, the impact of cerebral autoregulatory saturation was included, but the details of implementation were not. Nonetheless, this approach allows for clinically actionable explanations that do not depend on poorly understood mechanisms peripheral to the component being modeled, and provides a framework for systematically refining such models using a similar (but presumably vastly more complex) combination of black and grey box models and physiology. Again, if new tradeoffs not considered here are found to be significant, they can be added directly as additional constraints are recognized and solutions recomputed. (Further, tradeoffs may well change as organ systems fail, when these models are extended to disease states.)

High Frequency HRV

The high frequency fluctuations in HR that are particularly large at low mean workloads and low HR cannot be explained by the simple fits or models above, and thus additional signals and mechanisms must be included that can be causally related to this setting. **Figs. 5-6** shed light on breathing as a cause of much of the high frequency HRV. **Fig. 5A** shows HR (red) during natural breathing at rest, with the optimal static fit $h(V)=b \cdot V+c$ where V (blue) is measured ventilation flow

rates (inhalation and exhalation) at the mouthpiece. The static linear fit can be used to scale the units of V (blue) in **Fig. 5A** to visualize the best fit to HR (red) and its error, shown in Table 2. That HR and ventilation match so well in frequency (if not magnitude) is consistent with the observation that under certain conditions, inspiration is accompanied by an acceleration of heart rate, and expiration by a deceleration, a phenomenon called respiratory sinus arrhythmia (RSA) [38-45]. However, because ventilation and HR are both generated by neuroendocrine control, this fit (i.e. correlation) by itself does not suggest a specific mechanistic explanation of the resulting HR-ventilation correlation or HRV.

To sharpen this picture, **Fig. 6** shows data from subjects instructed to control respiratory rate (RR, shown in blue) by following a computer generated RR frequency sweep (tidal volumes not controlled), repeated with a background of 0 watt and 50 watts exercises respectively. (**Fig. 5B** shows HR and zoomed in for the 0 watt exercise data.) For each exercise taken separately, HR is fit with static (blue in **Fig. 5B**) and 1-state models, as well as a 2-state, 5-parameter linear model (shown in black in **Figs. 5B, 6, Table 2**)

$$\begin{aligned}\Delta h(t) &= a_1 h(t) + b_1 V(t) + x(t) \\ \Delta x(t) &= a_2 x(t) + b_2 V(t) + c\end{aligned}\tag{5}$$

where V is ventilatory flow rates, x is an internal “black box” state, and the parameters depend on workload. While breathing cannot be varied as systematically and widely as workload, these black-box fits provide strong evidence that ventilation is the main factor causing high frequency HRV. The underlying physiological mechanisms remain unclear, but we now know where to look next. In **Fig. 6**, minute ventilation naturally increases at 50 watts, yet HRV goes down, a nonlinear pattern consistent with the trends in **Figs. 1, 3**, but more dramatic. As **Table 2** shows, dynamic fits have little benefit for natural breathing at rest, but modestly reduce the error for the controlled respiratory sweeps at low and high frequency breathing. In all cases, HR frequency is fit better than the magnitude of the HR oscillations, suggesting both a dynamic and nonlinear dependence of HR on ventilatory flow rates.

Though RSA magnitude has been used as a measure of vagal function, after many years of research, the mechanism of RSA, e.g. whether RSA is due to a central or a baroreflex mechanism, is still debated [38-45]. Moreover, the data and dynamic fits show a small resonant peak in the frequency response at around 0.1 Hz at 0 watts, and the significance of the peak is unclear. Of note, this characteristic peak occurred in the fits for every subject (though the exact RR at which it occurs varied),

and is consistent with observations in the literature [38, 39]. (In SI, we also use both workload and ventilation data as inputs to fit HR data during the easy workout in the **Fig. 1**.)

Resolution of these mysteries requires additional measurements such as arterial blood pressure (more invasive human studies), more sophisticated physiological modeling including the mechanical effects of breathing on arterial blood pressure and pulmonary stretch reflexes, plus changing tradeoffs in control of arterial blood pressure at different watts and HR levels. In particular, Model (5) above assumed continuous ventilation and heart rates (i.e. no intra-breath or -beat dynamics), so more detailed modeling of physiological respiratory patterns and their mechanical and metabolic effects is needed.

Discussion:

Robust efficiency and actuator saturation

We showed how heart rate fluctuations in healthy athletes can be largely explained as nonlinear dynamic, but not chaotic, responses to either external (e.g. workload) or internal (e.g. ventilation implemented by pulsatile breathing) disturbance. We provided mechanistic explanations and plausible conjectures for essentially all the HRV in **Fig. 1**, and showed that changes in HRV per se, no matter how measured, are much less important mechanistically than the tradeoffs that produce them. The tradeoffs we highlight between robustness, homeostasis, and metabolic efficiency are universal and essential [1, 22] features of complex systems but can remain hidden and cryptic [46] without an appropriate mathematical framework [4, 47]. “Universal” features illustrated by this physiological (HR) control system include how efficiently maintaining robust homeostasis (e.g. small errors in CBF, S_aO_2 , and ΔO_2) in the presence of large disturbances requires correspondingly large actuator (e.g. HR, ventilation, and cerebral autoregulation) responses to compensate, and how nonlinearities in actuator saturations lead to reductions in actuator activity (e.g. HRV) under increased load or stress.

HR control and HRV highlight layered control, actuator constraints, and hard tradeoffs of the type that pervade physiology and are generally fundamental in complex control systems. In summary, actuators are the mechanisms by which controllers act on the system to provide efficient performance and robust homeostasis. In the cardiovascular models so far, the most important saturation is in cerebral autoregulation, which forces a nonlinear change in $H=h(W)$ as workload increases in order to avoid high P_{as} that leads to intracerebral pathology (edema, hemorrhagic stroke).

Further understanding of control complexity and the role of actuator (e.g. heart rate) variability and saturation in physiologic control comes from examination of other technological examples of complex systems. Familiar examples include automobiles, particularly new autonomous robotic versions.

A car is moved and controlled via the actuators that produce and deliver power, braking, and steering that result in accelerations in forward, backward, and lateral directions. Most complexity in an autonomous robot car is in the control system needed for robust efficiency to uncertainty in real traffic environments and to intrinsic variability in components. If scientists were forced to “reverse engineer” such a car without access to the forward engineering process, they would likely study “knockouts” of components to infer their function, and also push the vehicles to extremes to find the limits of their robust performance. It would be surprising if “reverse engineering” cardiovascular control would be easier than a robot car, or could be accomplished with less sophisticated tools and without domain specific details.

Loss of car actuator variability due to ‘stress’ parallels loss of HRV, in that it is loss of actuator *responsiveness* that causes deterioration of function, and loss of variability is only a symptom of actuator dysfunction. Currently, human drivers cause most crashes when they reduce their actuator responsiveness because of multitasking, alcohol consumption, fatigue, or poor visibility, or when surface conditions make the actuators less effective. Automatic collision avoidance and anti-lock and anti-slip traction control systems mitigate these effects, and augment human control in emergencies. But even in fully automated robotic cars with robust control systems, at extremes of speed, acceleration, braking, and turning (such as a race scenario or in icy conditions), actuators would frequently saturate and lose variability, resulting in less maneuverability, and an increase in errors and risk of crashes. Malfunctions in sensing or computing could also lead to loss of actuator responsiveness and thus loss of variability. Thus actuator saturation causing changes in variability is a “signature” of a wide variety of dangerous scenarios, and essential to understanding vehicle limits and malfunction. However, variability per se is unimportant, and analyzing the statistics of individual signals (e.g. fuel or air rates, braking, acceleration, turning rate, etc) in isolation is relatively less diagnostic compared to understanding integrated, mechanistic dynamic models of signal interactions.

Similar tradeoffs to those resulting in HRV are found throughout technology and biology. For example glycolytic oscillations were one of the most persistent mysteries involving dynamics in cell biology [1]. The proximal role of how autocatalytic and regulatory feedbacks make oscillations possible was well understood, but the unresolved deeper “why” question was the purpose of the oscillations, or alternatively, whether they were just frozen accidents of evolution. Oscillations are neither functional nor accidental but are a side effect of provably hard tradeoffs involving efficiency and robust control [1]. The glycolysis circuit must maintain adequate ATP concentrations that are robust to fluctuations in

demand and to enzyme and other metabolite levels. It must also be metabolically efficient, in the sense of not requiring excessive enzyme concentrations. Any circuit that aims to balance these competing requirements has the potential to oscillate, particularly when enzymes saturate.

Mathematical framework

It has been difficult to characterize multi-layered aspects of biological control, but our approach is aimed at providing tools for biologists and clinicians, combining established principles of system identification fits and control theory with basic physiological models. The fits in **Figs. 1, 5-7** highlight causal input-output relationships between variables and help suggest the relevant physiology. By comparison, even the most sophisticated statistical analysis of individual HR signals taken out of physiologic context is mechanistically uninformative. In contrast, the static and dynamic models mechanistically explain **Figs. 3, 4** and most of the variability in **Fig. 1** (i.e. the black curves at the lower two watts). Our explanation in terms of aerobic metabolism is simple and intuitive as well as mechanistic, and requires only basic mathematics and physiology. The main requirement of the models is some mechanistic relationship between control actuation and its limits in maintaining robust homeostasis. Thus we did not need detailed understanding of neuroendocrine control implementation or peripheral autoregulation, but only that they adequately manage the tradeoffs and saturation effects in muscle, brain, and heart as described above. Moreover, specific details of the computational approach, e.g. piecewise linear least squares used in this paper, are not essential to understanding the underlying system control. What is important is that the right constraints are properly reflected in the computation, so that the resulting controller function is constrained by the right physiological mechanisms plus appropriately changing penalties/constraints on vital physiological variables due to metabolic tradeoffs and limit.

Our approach also importantly highlights where mechanisms are missing. The model in (2,4) and **Fig. 4** does not capture any of the higher frequency HRV at low watts or the slow dynamics of anaerobic metabolism at high watts in **Fig. 1**. But taken together, the fits in **Figs. 5-7** suggest that dynamics of the mechanics of breathing and the chemistry of anaerobic muscle metabolism are necessary and perhaps sufficient to explain the rest of the HRV seen in **Fig. 1**. Model (2,4) assumed aerobic metabolism and continuous ventilation and heart rates (i.e. no intra-breath or -beat dynamics), so more detailed modeling of physiological respiratory patterns and their mechanical and metabolic effects is needed, as well as anaerobic metabolism at high workloads. There may also be connections between

robust efficiency and oscillations as in [1] to explain the origin of the peaks in frequency response of the breath-to-HR fits.

An essential feature of this project is that our tools be robust and scalable to more complex signals and models, and that if new mechanisms and/or tradeoffs are discovered that are important, they can be added as additional constraints. This aspect of modeling has been increasingly emphasized [47]. Fortunately, we can leverage enormous recent advances in engineering theory and practice, although these remain largely unknown in mainstream science outside of the most advanced parts of systems biology. The general models and methods, particularly moving from (1) to (2,3,4) (and **Fig. 1** to **Figs. 3-4**), used for this relatively straightforward study should serve well as a foundational framework for the evaluation of even more complex physiologic (disease) situations in which the diagnostic possibilities are broader.

Clinical Correlates: Linking the behavior of Control Systems and Pathophysiology

Clinicians know that changes in actuator signals (e.g. HR increases) can signify a great variety of potentially important derangements such as hypovolemia, congestive heart failure, inflammation, sepsis, etc [6-10]. Even without specific diagnostic content, alerts to clinicians that HRV is changing can be useful. Such an alert incorporated into monitoring of premature neonates prompts clinicians to suspect and treat sepsis (a major cause of mortality in this population), before more standard indications are detected [10]. This particular example of integration of mathematical analysis into monitors represents a special situation since the alert also incorporates the occurrence of cardiac decelerations, an event not observed in adults, and only one diagnosis is considered--sepsis, with only one treatment under consideration--antimicrobials. However, in most clinical scenarios, actuator changes alone are usually so generic that they lack specific diagnostic value, and extensive analyses of individual time series have not yielded mechanistic explanations that can narrow the diagnosis [6-9].

In contrast, the general type of models and methods used here and the application of control theory to physiology present an enormous opportunity to re-examine this area with powerful mathematical tools and a systems engineering approach [47]. This is important because system dysfunction is manifested earlier in the behavior of the control system than in any metric associated with the system's output. The long-term goal of this research is earlier diagnosis afforded by monitoring control elements in addition to individual signal outputs.

Materials and Methods

After Caltech Institutional Review Board approval, five fit athletic subjects (ages 25 to 35, 3 men and 2 women) performed a series of experimental exercise regimens, each on two different days. The intensity and durations were less than routine training for these athletes, and they had used the lab equipment before so were familiar and comfortable with the environment. In all experiments, the subject peddled a Life Fitness stationary recumbent bicycle at near constant speed with the peddling resistance controlled by a preprogrammed protocol. In the respiration rate (RR) sweep experiments, a sinusoid signal was preprogrammed in the computer with frequency from 2 Hz to 0.06 Hz and each subject watched the signal and controlled RR to follow the frequency of the signal until they were unable to continue.

In all exercise tests, 1 Hz work rate data were recorded from a Life Fitness stationary recumbent exercise bicycle interfaced with a computer running MATLAB via the CSAFE protocol. Other exercise testing data were collected using commercially available noninvasive monitors. (i) R-R interval HR data were recorded with a Polar heart rate monitor (Oulu, Finland) and converted to 1Hz HR data using a spline IPFM scheme [48]. (ii) In the tests shown in **Figs. 5, 6**, 100Hz ventilation (inhalation and exhalation) flow rate data were recorded with a Philips NiCO[®]2 Monitor, and down-sampled to 1Hz ventilation flow rate data. (iii) In the test shown in **Fig. 7**, 1Hz gas data including minute ventilation \dot{V}_E , oxygen consumption $\dot{V}O_2$ and carbon dioxide generation $\dot{V}CO_2$ were collected with a Vacumetrics monitor and TuboFitTM software (Ventura, CA). No other preprocessing of data was performed.

A detailed discussion of mathematical methods is given in SI.

Acknowledgements

We thank Pamela B. Pesenti for her gift in establishing the John G Braun Professorship, which supported this research, and Philips for providing equipment used in the experiments. The theoretical aspects of this work and the connections with other complex systems challenges were supported in part by AFOSR and NSF. Preliminary exploration in this research direction was funded by Pfizer, NIH (R01 GM078992), and the Institute of Collaborative Biotechnologies (ARO W911NF-09-D-0001). The research progress has been presented and discussed at several meetings, including the International Conference on Complexity in Acute Illness (ICCAI) of the Society for Complexity in Acute Illness (SCAI). Comments from many SCAI members greatly influenced this paper. We would also like to thank the athletes who were the subjects for this study.

References and Notes

1. Chandra, F.A., G. Buzi, and J.C. Doyle, *Glycolytic Oscillations and Limits on Robust Efficiency*. Science, 2011. **333**(6039): p. 187-192.
2. Pool, R., *Is it healthy to be chaotic?* Science, 1989. **243**(4891): p. 604-607.
3. Buzsáki, G., *Rhythms of the Brain*. 2006: Oxford University Press, USA.
4. Glass, L., *Synchronization and rhythmic processes in physiology*. Nature, 2001. **410**: p. 277-284.
5. Buchman, T.G., *The community of the self*. Nature, 2002. **420**: p. 246-251.
6. Goldberger, A.L., et al., *Fractal dynamics in physiology: alterations with disease and aging*. Proceedings of the National Academy of Sciences of the United States of America, 2002. **99**(Suppl 1): p. 2466-2472.
7. Camm, A.J., et al., *Heart Rate Variability: Standards of measurement, physiological interpretation, and clinical use*. Circulation, 1996. **93**(5): p. 1043-1065.
8. Ivanov, P.C., et al., *Multifractality in human heartbeat dynamics*. Nature, 1999. **399**: p. 461-465.
9. Poon, C.S. and C.K. Merrill, *Decrease of cardiac chaos in congestive heart failure*. Nature, 1997. **389**: p. 492-495.
10. Moorman, J.R., et al., *Cardiovascular oscillations at the bedside: early diagnosis of neonatal sepsis using heart rate characteristics monitoring*. Physiologic Measurement, 2011. **32**(11): p. 1821-1832.
11. Tulppo, M.P., et al., *Quantitative beat-to-beat analysis of heart rate dynamics during exercise*. American Journal of Physiology-Heart and Circulatory Physiology, 1996. **271**(1): p. H244-H252.
12. Yamamoto, Y., R.L. Hughson, and J.C. Peterson, *Autonomic control of heart rate during exercise studied by heart rate variability spectral analysis*. Journal of Applied Physiology, 1991. **71**(3): p. 1136-1142.
13. Akselrod, S., et al., *Power spectrum analysis of heart rate fluctuation: a quantitative probe of beat-to-beat cardiovascular control*. Science, 1981. **213**(4504): p. 220-222.
14. Mackey, M.C. and L. Glass, *Oscillation and chaos in physiological control systems*. Science, 1977. **197**(4300): p. 287-289.
15. Searching Google Scholar with the exact phrase “heart rate variability” for just 2011 returns 695 papers with the phrase in the title and 9330 anywhere in the paper, of which 891 have at least one of the following words: chaos, chaotic, or fractal.
16. Barabási, A.L., *Scale-free networks: a decade and beyond*. Science, 2009. **325**(5939): p. 412-413.

17. Glass, L., *Introduction to controversial topics in nonlinear science: Is the normal heart rate chaotic?* Chaos, 2009. **19**(2): p. 28501.
18. Kluttig, A., O. Kuss, and K. Greiser, *Ignoring lack of association of heart rate variability with cardiovascular disease and risk factors:: Response to the manuscript.* International journal of cardiology, 2010. **145**(2): p. 375-376.
19. Ioannidis, J.P.A., *Why most published research findings are false.* PLoS medicine, 2005. **2**(8): p. e124.
20. Young, N.S., J.P.A. Ioannidis, and O. Al-Ubaydli, *Why current publication practices may distort science.* PLoS medicine, 2008. **5**(10): p. e201.
21. Stumpf, M.P.H. and M.A. Porter, *Critical Truths About Power Laws.* Science, 2012. **335**(6069): p. 665-666.
22. Alderson, D.L. and J.C. Doyle, *Contrasting views of complexity and their implications for network-centric infrastructures.* Systems, Man and Cybernetics, Part A: Systems and Humans, IEEE Transactions on, 2010. **40**(4): p. 839-852.
23. Wigertz, O., *Dynamics of ventilation and heart rate in response to sinusoidal work load in man.* Journal of Applied Physiology, 1970. **29**: p. 208-218.
24. Warner, H.R. and A. Cox, *A mathematical model of heart rate control by sympathetic and vagus efferent information.* Journal of Applied Physiology, 1962. **17**(2): p. 349-355.
25. Brooks, G.A., T.D. Fahey, and T.P. White, *Exercise physiology: human bioenergetics and its applications.* 1996: Mayfield publishing company.
26. Rowell, L.B., *Human cardiovascular control.* 1993: Oxford University Press, USA.
27. Grodins, F.S., J. Buell, and A.J. Bart, *Mathematical analysis and digital simulation of the respiratory control system.* Journal of Applied Physiology, 1967. **22**(2): p. 260-276.
28. Guyton, A. and J. Hall, *Textbook of medical physiology. 11th Edn.* 2006, Philadelphia,USA: Elsevier Saunders Co.
29. Hoppensteadt, F.C. and C.S. Peskin, *Modeling and simulation in medicine and the life sciences.* 2002: Springer Verlag.
30. Batzel, J.J. and D. Schneditz, *Cardiovascular and respiratory systems: modeling, analysis, and control.* 2007: Society for Industrial Mathematics.
31. Ljung, L., *System identification: theory for the user.* 1987: Prentice-Hall NJ.

32. Murray, R.M., *Optimization-Based Control*.
Preprint: <http://www.cds.caltech.edu/~murray/amwiki/index.php?title=Supplement: Optimization-Based Control>, 2008.
33. Todorov, E., *Optimal Control Theory*. Bayesian Brian, 2006.
34. Cheng, T.M., et al., *Nonlinear modeling and control of human heart rate response during exercise with various work load intensities*. Biomedical Engineering, IEEE Transactions on, 2008. **55**(11): p. 2499-2508.
35. Mullen, T.J., et al., *System identification of closed-loop cardiovascular control: effects of posture and autonomic blockade*. American Journal of Physiology-Heart and Circulatory Physiology, 1997. **272**(1): p. H448-H461.
36. Paulson, O., S. Strandgaard, and L. Edvinsson, *Cerebral autoregulation*. Cerebrovascular and brain metabolism reviews, 1990. **2**(2): p. 161-192.
37. Bramble DM and L. DE, *Endurance running and the Evolution of Homo*. Nature, 2004. **432**(7015): p. 345-352.
38. Mehlsen, J., et al., *Heart rate response to breathing: dependency upon breathing pattern*. Clinical Physiology, 1987. **7**(2): p. 115-124.
39. Novak, V., et al., *Influence of respiration on heart rate and blood pressure fluctuations*. the American Physiological Society, 1993: p. 617-626.
40. Hirsch, J. and B. Bishop, *Respiratory sinus arrhythmia in humans: how breathing pattern modulates heart rate*. the American Physiological Society, 1981: p. 10.
41. Eckberg, D.L., *Human sinus arrhythmia as an index of vagal cardiac outflow*. Journal of Applied Physiology, 1983. **54**(4): p. 961-966.
42. Schäfer, C., et al., *Heartbeat synchronized with ventilation*. Nature, 1998. **392**: p. 239-240.
43. Grossman, P., J. Karemaker, and W. Wieling, *Prediction of tonic parasympathetic cardiac control using respiratory sinus arrhythmia: the need for respiratory control*. Psychophysiology, 1991. **28**(2): p. 201-216.
44. Berntson, G.G., J.T. Cacioppo, and K.S. Quigley, *Respiratory sinus arrhythmia: Autonomic origins, physiological mechanisms, and psychophysiological implications*. Psychophysiology, 1993. **30**(2): p. 183-196.

45. Eckberg, D.L., *Point: counterpoint: respiratory sinus arrhythmia is due to a central mechanism vs. respiratory sinus arrhythmia is due to the baroreflex mechanism*. Journal of Applied Physiology, 2009. **106**(5): p. 1740-1742.
46. Doyle, J. and M. Csete, *Architecture, constraints, and behavior*. PNAS, 2011. **108**(Supplement 3): p. 15624-15630.
47. Winslow, R.L., et al., *Computational medicine: translating models to clinical care*. Science Translational Medicine, 2012. **4**(158): p. 158rv11.
48. Han, K., J.H. Nagel, and N. Schneiderman, *A continuous representation of heart rate*. Engineering in Medicine and Biology Society, 1992 14th Annual International Conference of the IEEE, 1992. **2**: p. 785-786.

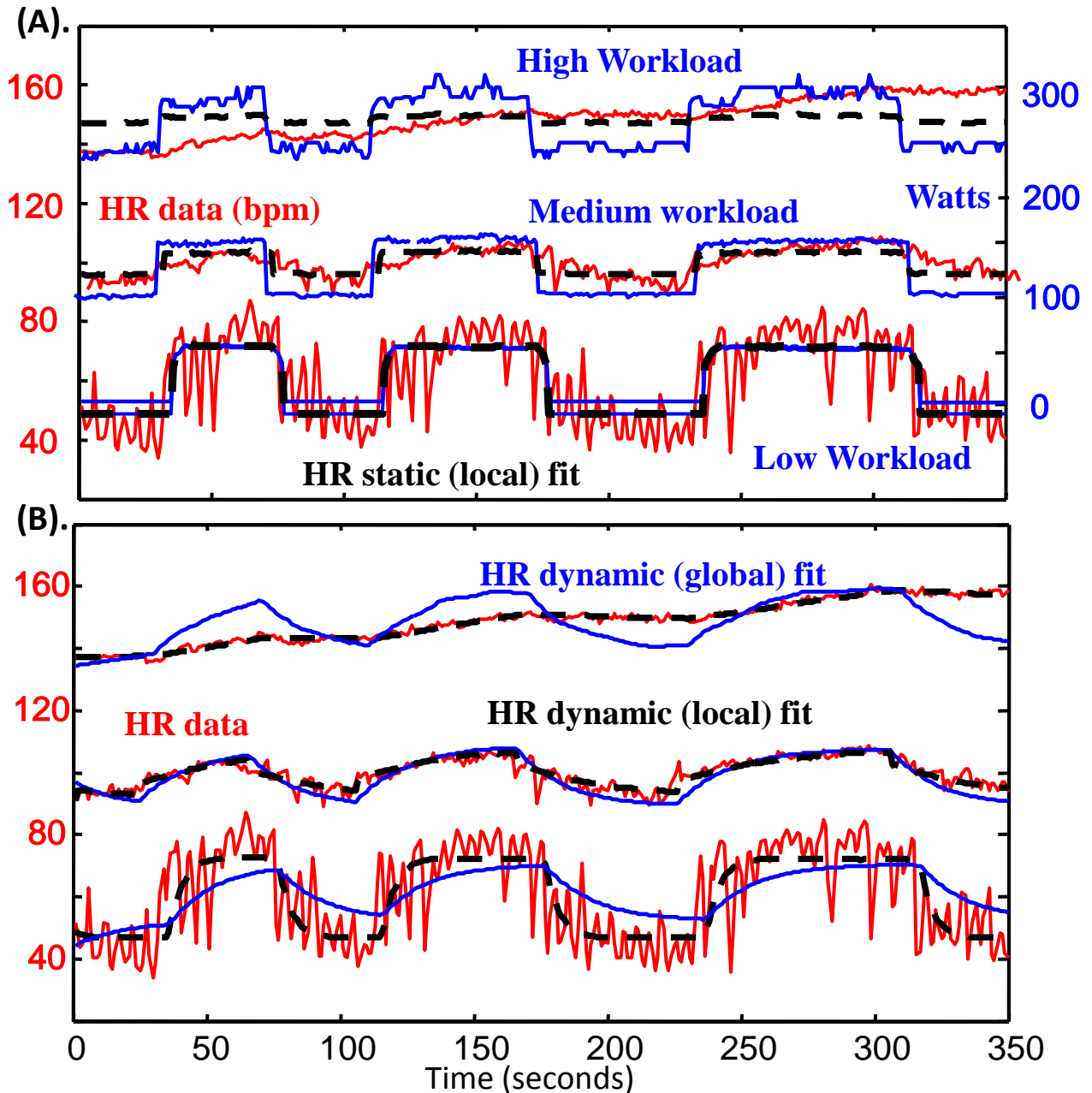


Figure 1: HR responses to simple changes in muscle work rate on a stationary bicycle: Each experimental subject performed separate stationary cycle exercises of ~ 10 minutes for each workload profile, with different means but nearly identical square wave fluctuations around the mean. A typical result is shown from subject #1 for 3 workload profiles with time on the horizontal axis (zoomed in to focus on a 6 minute window). (A) HR (red) and workload (blue); linear local piecewise static fits (black) with different parameters for each exercise. The workload units (most strenuous exercise on top of graph) are shifted and scaled so that the blue curves are also the best global linear fit. (B) Corresponding dynamics fits, either local piecewise linear (black) or global linear (blue). Note that, on all time scales, mean HR increases and variability (HRV) goes down with the increasing workload. Breathing was spontaneous (not controlled).

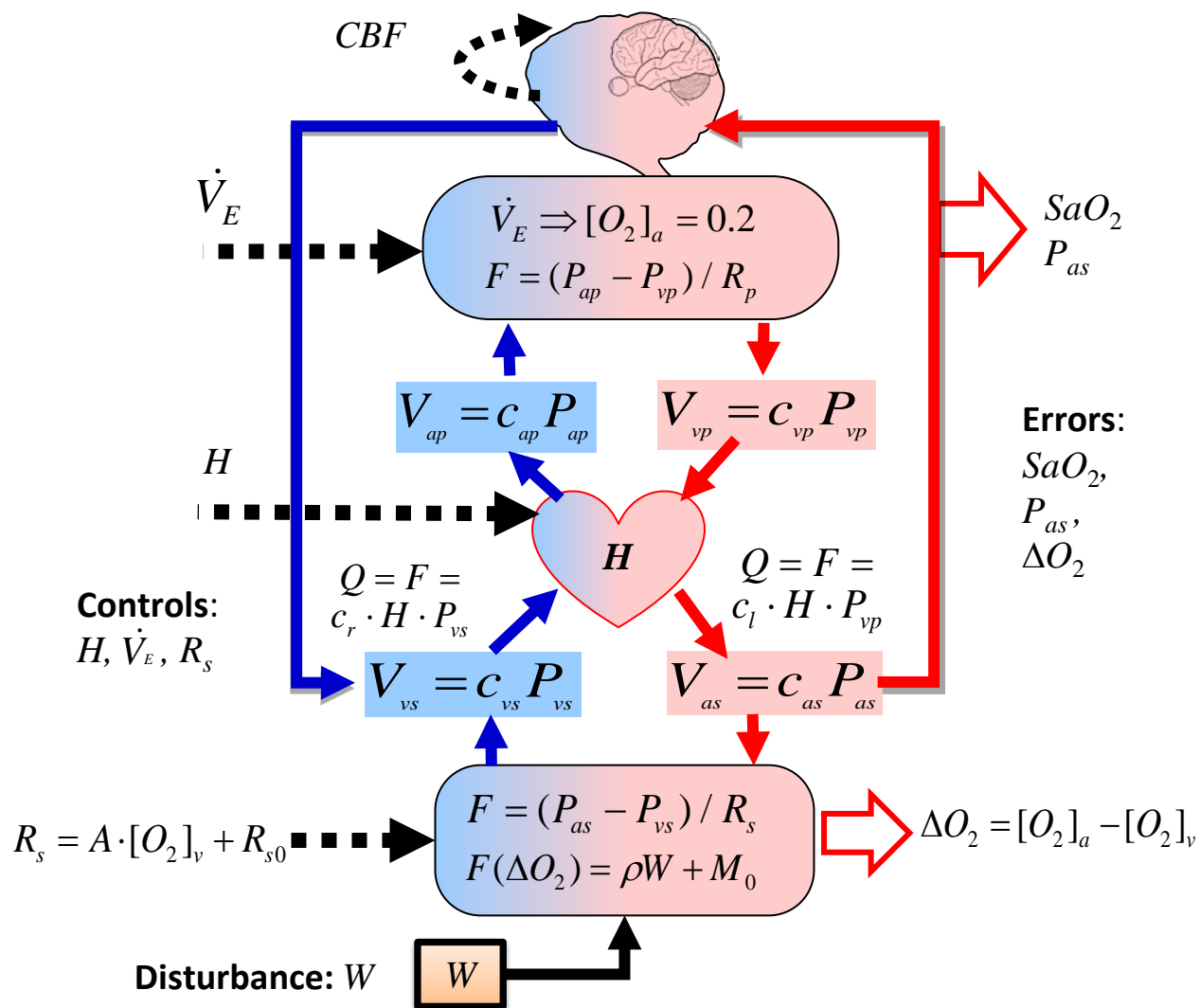


Figure 2: Schematic for cardiovascular control of aerobic metabolism and summary of main variables: Blue arrows represent venous beds, and red arrows are arterial beds, and dashed lines represent controls. Four types of signals, distinct in both functional role and time series behavior, together define the required elements for robust efficiency. The main control requirement is to maintain 1) small “errors” in internal variables for brain homeostasis (e.g., arterial O_2 saturation SaO_2 , mean arterial blood pressure P_{as} , and cerebral blood flow CBF), and muscle efficiency (oxygen extraction ΔO_2 across working muscle) despite 2) external disturbances (muscle work rate W), and 3) internal sensor noise and perturbations (e.g. pressure changes from different respiratory patterns due to pulsatile ventilation V) using 4) actuators (heart rate H , minute ventilation \dot{V}_E , vasodilatation and peripheral resistance R , and local cerebral autoregulation).

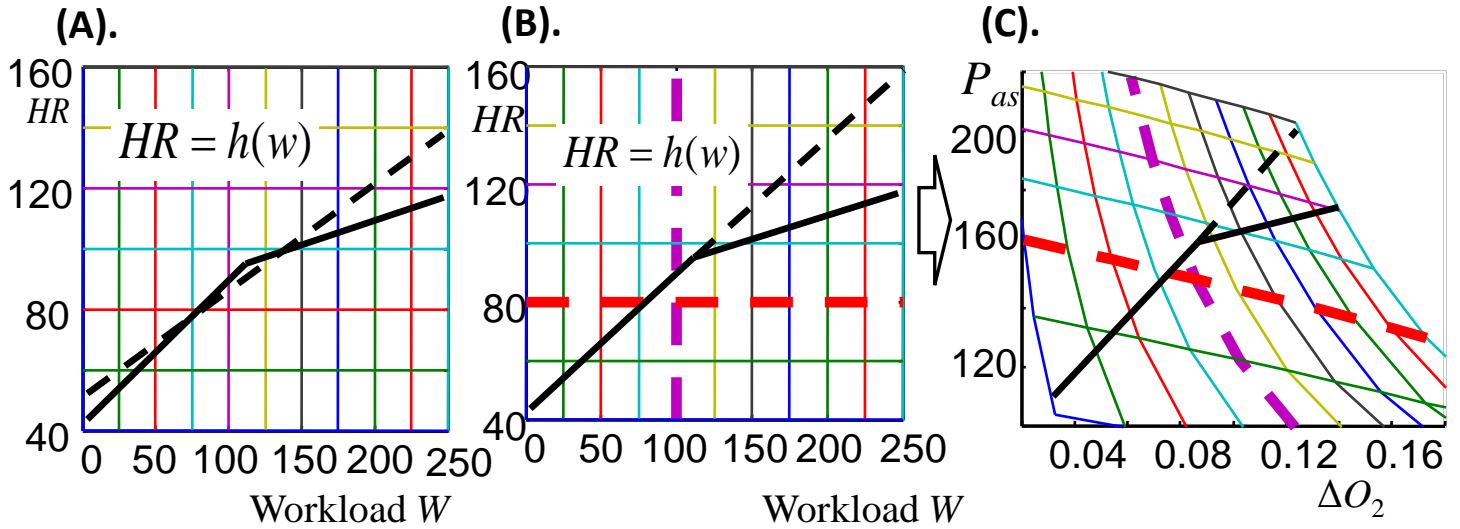


Figure 3: Static analysis of cardiovascular control of aerobic metabolism as workload increases: Static data from Fig. 1A are summarized in (A) and the physiological model explaining the data is in (B) and (C). The solid black curves in (A) and (B) are idealized (i.e. piecewise linear) and qualitatively typical values for $H=h(W)$ that are globally consistent with static piecewise linear fits (black in Fig. 1A) at the two lower workload levels. The dashed line in (A) shows $h(W)$ from the global static linear fit (blue in Fig. 1A) and in (B) shows a hypothetical but physiologically implausible linear continuation of increasing HR at the low workload level (solid line). The mesh plot in (C) depicts P_{as} - ΔO_2 (mean arterial blood pressure -- tissue oxygen difference) on the plane of the H - W mesh plot in (B) using the physiological model $(P_{as}, \Delta O_2) = f(H, W)$ for generic, plausible values of physiological constants. Thus any function $H=h(w)$ can be mapped from the H, W plane (B) using model f to the $(P, \Delta O_2)$ plane (C) to determine the consequences of P_{as} and ΔO_2 . The reduction in slope of $H=h(w)$ with increasing workload is the simplest manifestation of changing HRV addressed in this study.

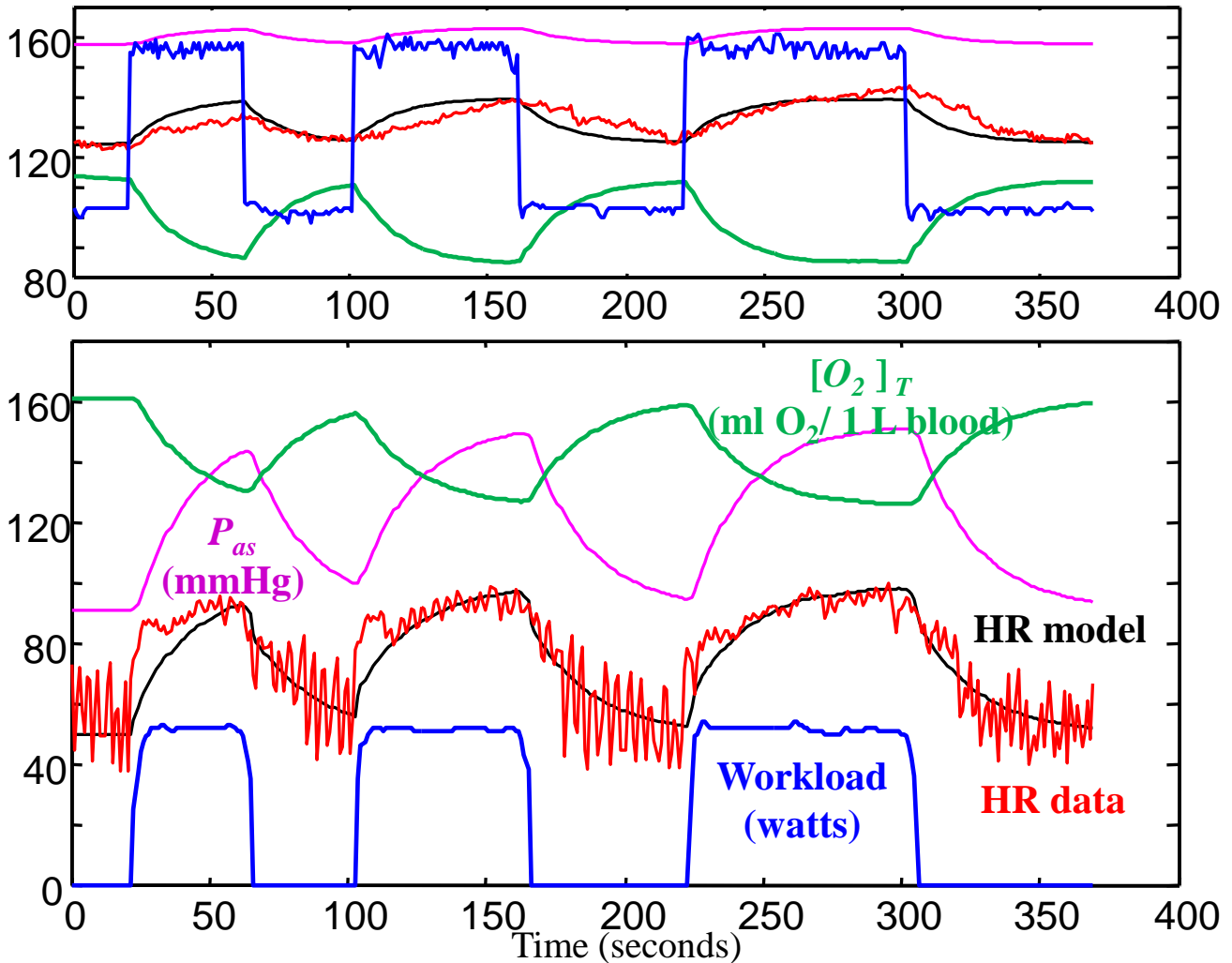


Figure 4: Optimal control model response using 1st principle model to two different workload (blue) demands, approximately square waves of 0-50 w (lower) and 100-150w (upper): For each data set (using Subject #2 data), a physiological model with optimal controller is simulated with workload as input (blue) and HR (black) as output, and compared with collected HR data (red). Simulations of blood pressure (P_{as} , purple) and tissue oxygen saturation ($[O_2]_T$, green) are consistent with the literature but data were not collected from subjects. Breathing is spontaneous (not shown).

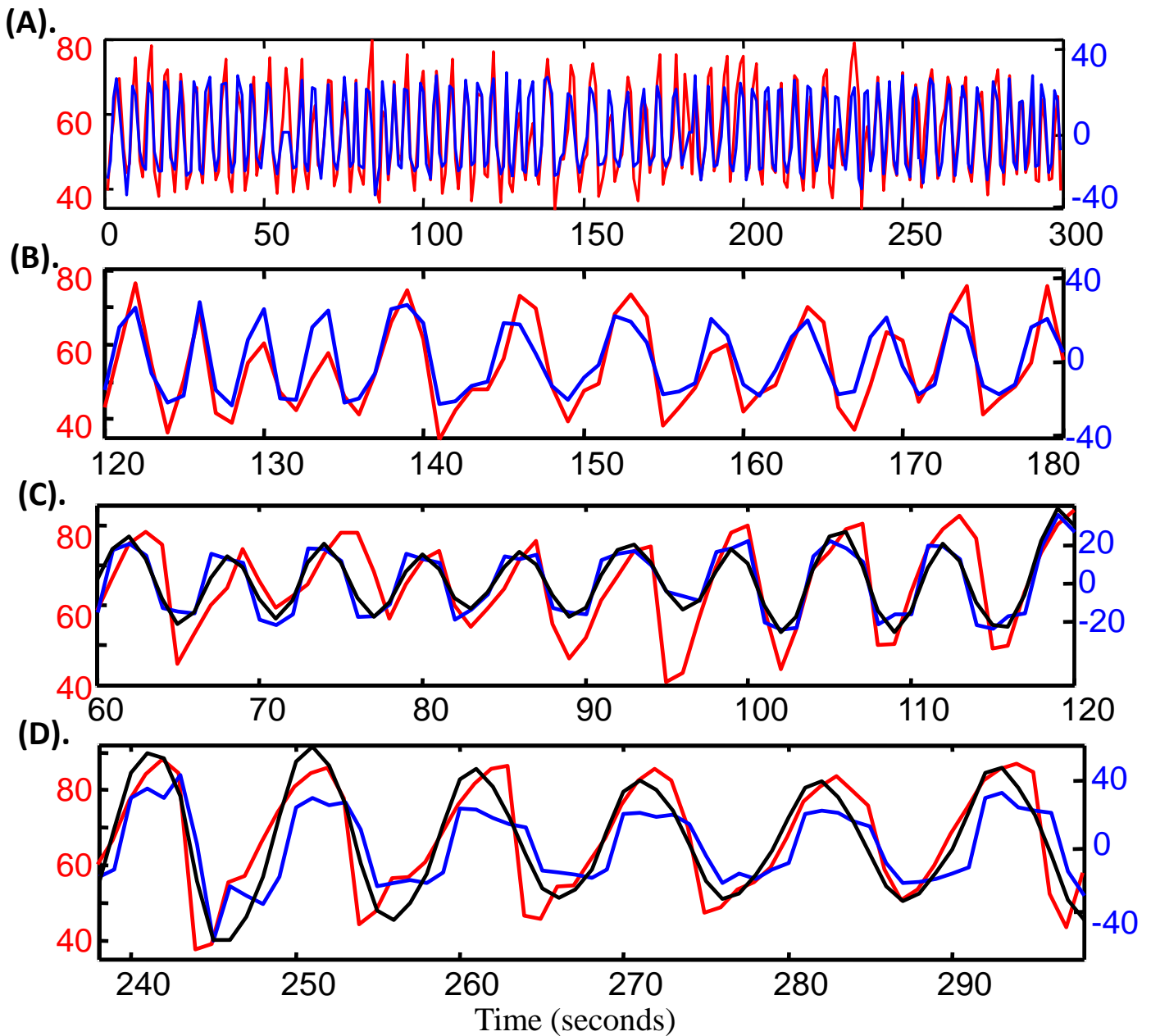


Figure 5: Heart rate response (red) to ventilation v (blue) at rest (0 watts): The ventilatory data are raw speed of inhalation and exhalation measured at the mouthpiece. In each case the units for v (blue) are chosen to show the optimal static fit $h(v)=b\cdot v+c$ to the collected HR data. **(A)** and **(B)** show natural breathing, with **(B)** zoomed in to focus on a smaller window to help visualize the data and fit. **(C)** and **(D)** are similar focused smaller windows from a longer controlled breathing experiment at resting (0 watts) where the subject followed a frequency sweep from fast to slow breathing (see Figure 6 for the full frequency range). **(C)** focuses on breathing frequencies close to natural breathing, while **(D)** focuses on frequencies slower than natural. Both **(C)** and **(D)** show simulated dynamic fits (black), and optimal static fits $h(v)=b\cdot v+c$ (blue). The dynamic fits improve on the static fits more for the controlled sweep than for natural breathing (see Table 2).

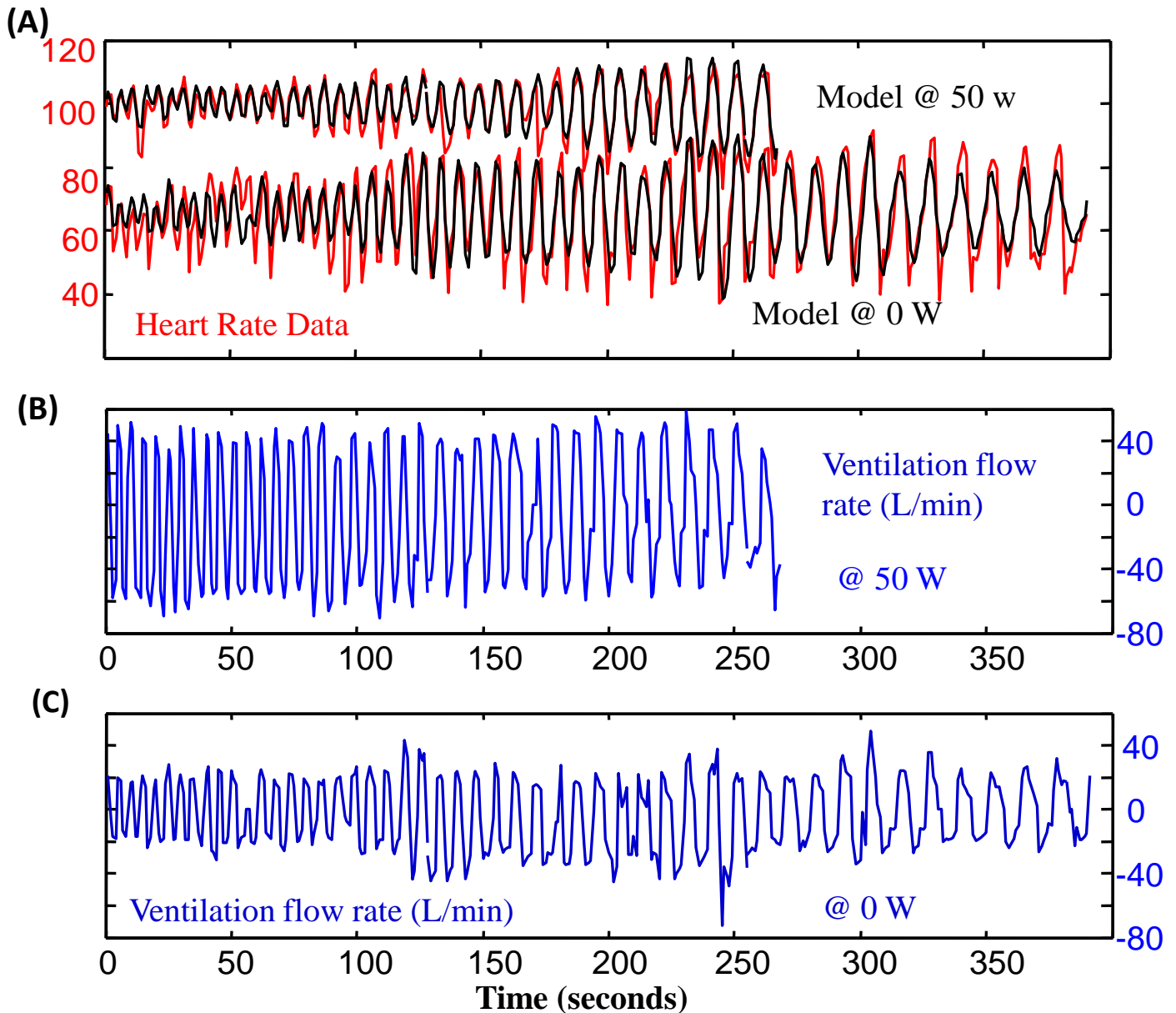


Figure 6: HR response to sweep ventilation on different workload levels: Two experiments with (A) HR (red) and dynamic fit (black) to input of controlled ventilation frequency sweeps with measured ventilatory flow rate (blue) on a fixed background workload of (B) 0 or (C) 50 watts. Ventilatory flow (with spontaneous ventilation magnitude) was necessarily larger at 50 watts and the subject was unable to breathe slowly enough to complete the entire frequency sweep.

Table 1: RMS error for models of different complexity for data in Figure 1. Items in yellow highlight the best models balancing fitting error with model complexity. For the piecewise model, $i=1,2,3$ stands for each exercise level respectively, i.e., 0-50, 100-150, 250-300 watts.

Row #	# prms	Model structure	0-50 watts	100-150 watts	250-300 watts
1	0	zero: $h(W)=0$	60.40	99.97	148.59
2	2	global static: $h(W)=b \cdot W+C$	10.1	6.9	10.4
3	3=1×3	piecewise constant $h_i(W)=C_i$	14.8	4.7	6.7
4	6=2×3	piecewise static $h_i(W)=b_i \cdot W+C_i$	9.6	3.2	6.6
5	3	global 1st order $\Delta h(t)=ah(t)+bW+C$	11.6	3.2	6.5
6	9=3×3	piecewise 1 st order $\Delta h_i(t)=ah_i(t)+b_iW+C_i$	8.9	2.1	0.9

Table 2: RMS error for models of different complexity for data in Figure 5-6. Items in yellow highlight the best models balancing fitting error with model complexity.

Row #	# prms	Model structure	Resting natural	Resting sweep	50 watts sweep
1	0	zero	56	67	98
2	1	constant	11.6	13.1	7.9
3	2	Static	6.4	9.7	5.9
4	3	1 st order dynamic	6.0	9.7	5.5
5	6	2 nd order dynamic	6.0	7.5	4.0